Exchange Anisotropy and Surface Crystallization in Annealed Cobalt-rich Amorphous Alloys

C. K. Kim and C. G Yoo

Division of Materials Science and Metallurgical Engineering,
Hanyang University Haengdang-Dong,
Seongdong-Ku, Seoul, 133-791 KOREA

비정질계 코발트 합금의 열처리시에 얻어지는 유도 이방성과 표면 결정화에 관한 연구

김 창 경, 유 충 근

한양대학교 재료공학부

Abstract

코발트계 비정질 합금을 여러 온도 구간 및 시간에 대해서 열처리하여 표면 결정화 현상이 자기 이방성에 미치는 영향을 탐구하였다. 자기 이방성은 비정질 표면의 결정 구조에 민감한 변화를 보였는데 면심입방점 코발트에 많은 결함이 존재할 경우 자기이방성이 최대치를 나타 내었다.

1. INTRODUCTION

A field-displaced $M-H$ loop (referred to as exhibiting exchange anisotropy) is generally ass℃iated with exchange coupling between two intimately contacting magnetic materials having very different coercivities. It is not obvious how to explain the appearance of exchange anisotropy in amorphous alloys heat treated well below their bulk crystallization temperature, T_x. Glancing angle X-ray diffraction from samples annealed at temperatures up to 400℃ showed a broad diffracted peak while TEM revealed striking microstructural features for samples annealed as low as 250 ℃. We have therefore used transmission electron microscopy (TEM) to obtain direct microstructural evidence of field annealing and early stages of crystallization in amorphous cobalt rich alloys. We describe what we believe to be the most detailed microscopic evidence to date of the micromechanisms of field annealing cobalt rich amorphous alloys.

2. EXPERIMENT

Amorphous $Co_{95-x}Fe_5(BSi)_x$ alloys were made by melt spinning. Compositions were verified by chemical analysis with Auger electron spectroscopy (AES), X-ray photoelectron spectroscopy (XPS) and electron probe microanalysis (EPMA). These compositions are cha-racterized by near-zero magnetostriction ($\lambda_s < 1 \times 10^{-6}$) and high d.c. permeability in the as-cast state. Differential scanning calorimetry indicates that crystallization starts at 465℃ and the crystallization peak maximum ℃curs at 535℃. Ribbons with a cross section of $20\mu m \times 2mm$ were cut to a length of 40mm. Samples were then field annealed (60 Oe w.r.t. a long ribbon axis) for various times (3min.-7hrs.), at different temperature (250℃-440℃) and in air or flowing dry nitrogen. Maximum annealing temperature was set well below the temperature for the onset of crystallization, 465℃.

M-H loops were taken on 40 mm single lengths of ribbon using a balance pair of opposing pickup coils and a loop tracer. Exchange coupling was measured as an offset (H_{offset}) in the hysteresis loop.

In order to obtain direct microstructural evidence of the early stages of crystallization and of field annealing, we used transmission electron microscopy (TEM) (JEOL 200 CX and Akashi 002B operating at 200 keV). Scanning TEM (STEM) observation was made using a VG HB5 FEG-STEM with LINK LZ-5 X-ray detector.

Several series of electron-transparent plan-view TEM specimens were prepared using a single or double gun argon ion milling method. Ion milling was performed in a liquid nitrogen cold stage to avoid possible beam heating. Electron microprobe analysis with STEM was used to obtain l℃al compositional information.

3. RESULT AND DISCUSSION

3.1 Magnetic measurements.

The alloys studied are listed in Table I. The field annealed ribbons showed coercivities in the range of 40 to 100 mOe (Fig. 1). The anisotropy field, of order 1 Oe, is due mainly to demagnetization of the 40 mm long samples. The loops also showed a weak exchange anisotropy as indicated in Fig. 1. The exchange anisotropy varies systematically with increasing annealing time and temperature (Fig. 2). Specimens field-annealed in nitrogen atmosphere did not exhibit any offset. The offset vanishes upon bulk crystallization of the ribbons (e.g. 10 min at 440℃). Exchange anisotropy in the loop of a soft magnetic material is generally caused by exchange coupling between the soft material and a hard or semi-hard component. The microstructural origin of this exchange anisotropy is of interest.

Table 1 Composition of the alloys studied.

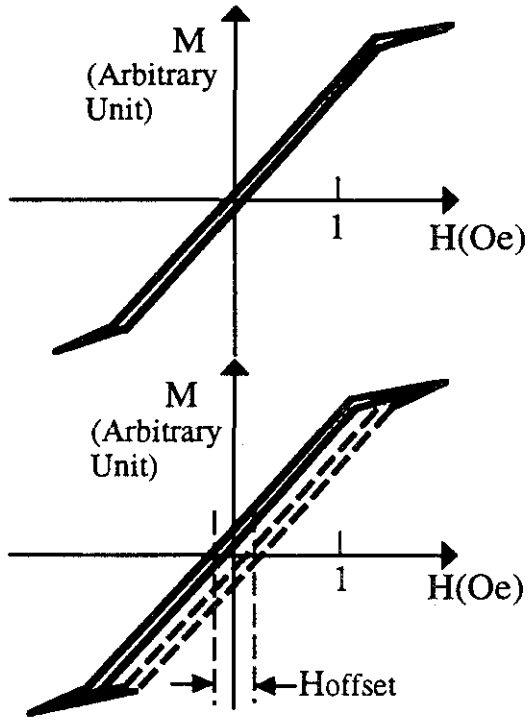| Material Designation	Alloy Composition (at%)
S-0 material	$Co_{74.26} Fe_{4.74} B_{21}$
S-2 material	$Co_{74.26} Fe_{4.74} Si_{2.1} B_{18.9}$
S-8 material	$Co_{74.26} Fe_{4.74} Si_{8.4} B_{12.6}$
S-10 material	$Co_{70.5} Fe_{4.74} Si_{10} B_{15}$
S-13 material	$Co_{74.26} Fe_{4.74} Si_{12.6} B_{8.4}$

Fig. 1 M-H loops of $Co_{74.26}Fe_{4.74}Si_{2.1}B_{18.9}$ amorphous ribbon after field annealing and ac demagnetization (upper) and after positive (solid curve) and negative (dashed curve) field pulses of order 200 Oe.

4. Surface oxide.

Amorphous $Co_{74}Fe_5B_{19}Si_2$ has a crystallization temperature of approximately 465℃. However, annealing in air at temperatures as low as 250℃ leads to the formation of a surface oxide. Our TEM/STEM investigations show the oxide at the surface of the ribbon to be nonmagnetic borosilicate $(B_2O_3+SiO_2)$ (Fig. 3). Electron diffraction patterns obtained from these oxides indicate that they retain amorphous structures. In the case of S-0 $(Co_{74}Fe_5B_{21})$ and S-2 $(Co_{74}Fe_5B_{19}Si_2)$ ribbons (refer to Table I
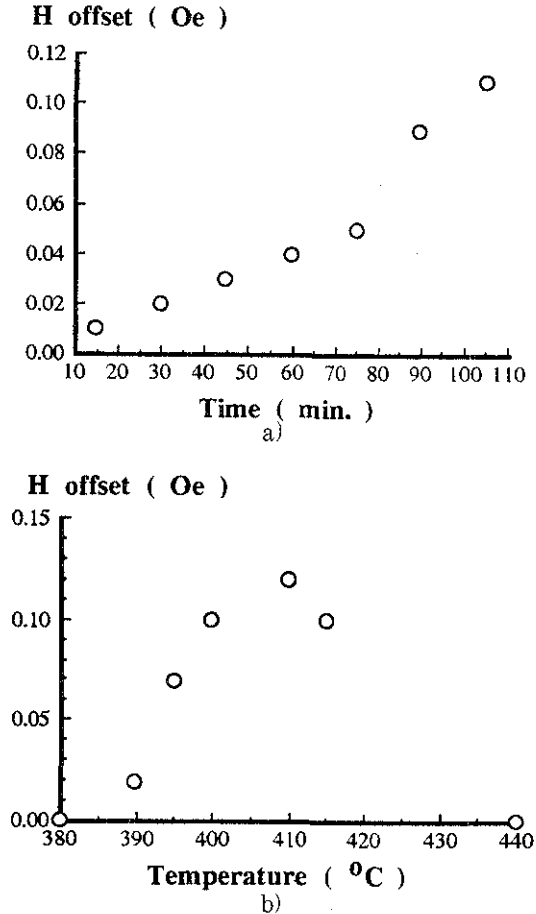

Fig. 2 a) Field annealing response of $Co_{74.26}Fe_{4.74}Si_{2.1}B_{18.9}$ amorphous ribbon (S-2 material) annealed at 380℃ for various duration of time.

b) Field annealing response of $Co_{74.6}Fe_{4.74}Si_{2.1}B_{18.9}$ amorphous ribbon (S-2 material) annealed for 10 min. at various temperatures.

for composition), the oxide is largely B_2O_3 type (determined by AES and STEM) and its diffraction pattern indicates only weak atomic correlations i.e. it is highly disordered and porous (Fig. 3a). In the S-13 ribbons, the oxide is predominantly SiO_2 with a compact structure showing more short range order in its electron diffraction pattern (Fig. 3b). The oxide
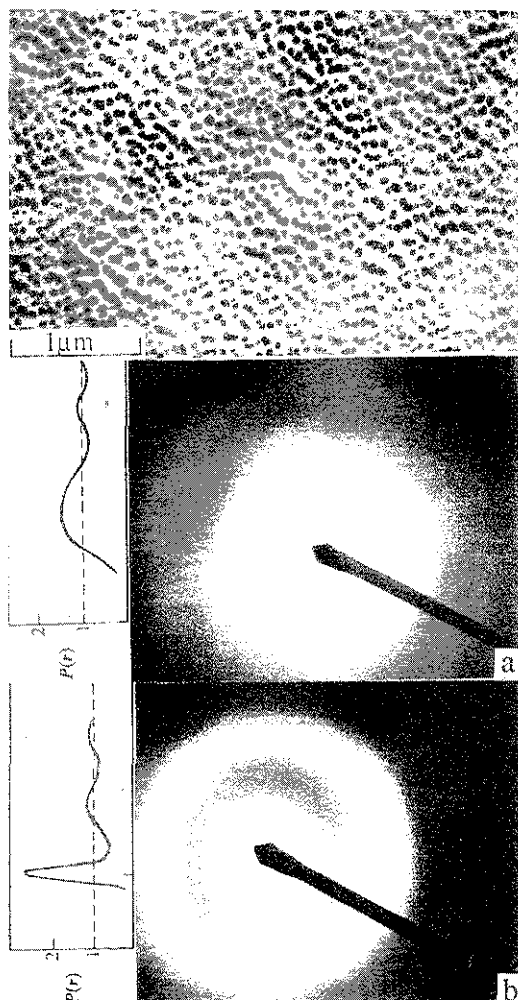
Fig. 3. TEM bright field image of the amorphous oxide formed on the crystallized substrate $Co_{74.28}Fe_{4.78}Si_{12.1}B_{14.9}$ (identified as S-2 material) during annealing at 380℃ for 60 min.

a) Diffraction pattern obtained from the oxide layer formed on S-2 material showing amorphous halo (Inset: schematic intensity distribution).

b) Diffraction pattern obtained from the oxide layer formed on S-13 material showing amorphous halo which shows a higher degree of spatial correlation compared to Fig. 3a. (Inset: schematic intensity distribution)

formed on the S-8 ribbon appears to possess an intermediate state of packing.

The formation of the surface oxide reduces the concentration of glass-stabilizing elements (B and Si) in a thin layer of the underlying amorphous alloy. This has been confirmed by in-situ microanalysis and Auger depth profile. This metalloid reduction leads to a decrease in the crystallization temperature T_x of the amorphous alloy just beneath the oxidized surface. Consequently, after sufficient time (e.g. 30 min at 380℃, well below the bulk T_x) a magnetic, crystalline, cobalt-rich layer (10 to 100 nm in thickness) forms beneath the oxidized surface.

5. Crystalline cobalt.

The microstructure of the cobalt layer in S-0 and S-2 ribbons consists of faulted nan℃rystalline Co with a face centered cubic structure (Fig. 4). That of S-13 ribbon was composed of unfaulted nan℃rystalline Co with a close packed hexagonal structure (Fig. 5). A mixture of hexagonal and cubic Co crystallites was observed in S-8 ribbons. Two distinctive microstructures appeared in S-10 ribbons: after low temperature anneal, oxidation governed the microstructure and the result was crystallization to hcp phase; at high temperature, thermodynamically stable fcc Co phases formed.

The striking microstructural feature we observed in the face-centered cubic metal phase is a high density of faults. The faulting was clearly demonstrated both in a real (Fig. 4a) and recipr℃al (Fig. 4b) space. In aggressively
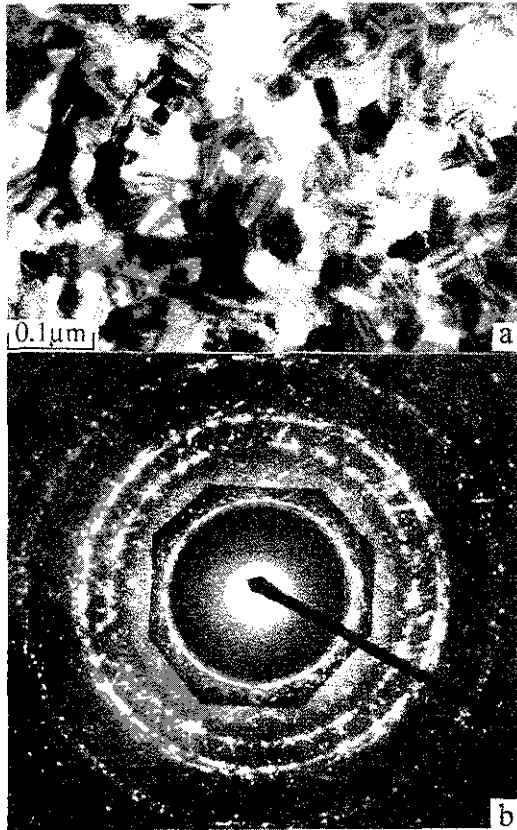
Fig. 4 a) TEM bright field images of the crystalli-
zed substrate $Co_{74.26}Fe_{4.74}Si_{3.1}B_{18.9}$ (identified
as S-2 material) during annealing at 380℃
for 60 min..
b) Diffraction pattern obtained from faulted
nano-crystallites. The position of the diffra-
cted maxima indicates that (200) diffracted
ring is missing from the fcc diffraction pat-
tern (See inset. Missing ring is indicated by
an arrow.).

Fig. 5 TEM bright field image of the crystallized
substrate $Co_{74.26}Fe_{4.74}Si_{12.6}B_{8.4}$ (identified as
S-13 material) during annealing at 380℃ for
60 min. (Inset : hcp diffraction pattern)

annealed samples, the ribbon surface was cov-
ered with highly faulted crystallites which ap-
pear to form on the {111} planes of fcc Co.
These faults consist of {111} planes of oxygen
atoms which interrupt the normal stacking of
planes of fcc Co along <111> directions. The
major source of oxygen for these faults is the
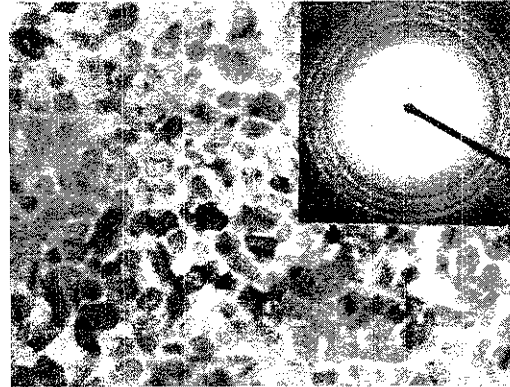atmosphere during annealing since samples

annealed in nitrogen did not show faulting.
Significant exchange anisotropy was observed
only in cases with strongly faulted fcc cobalt
layers.

6. Discussion

A {111} oxygen fault plane is locally coordi-
nated like a {111} oxygen plane in $CoOFe_2O_3$
spinel ferrite. This local spinel-like planar de-
fect probably has much stronger magnetic an-
isotropy energy associated with it (for cobalt
ferrite, $K_1 \approx 2.5 \times 10^5$ J/m^3) than does the par-
ent alloy (for Perminvar, $K_1 \approx 10^3$ J/m^3 and for
Permalloy or amorphous Co-rich alloys, $K_1 \approx 10^2$
J/m^3). The details of how the oxygen faults
affect exchange coupling are unclear.

This new mechanism of exchange anisotropy
which we have found to operate in cobalt-rich
amorphous alloys appears to be similar to that
identified by Heidenreich and Nesbitt[1] to be
responsible for field annealing in crystalline
Co-Ni-Fe (Permendur and Permalloy) alloys

and field-induced ordering in Ni_3Fe by Nesbitt et al.[2]. We speculate that the faulted surface crystallized layer acts like a semi-hard magnet that is exchange coupled to the interior of the ribbon. As the surface crystallization and faulting increases, the exchange coupling increases.

We can estimate the exchange field[3] due to such a thin layer of semi-hard cobalt in contact with the amorphous ribbon of thickness t_a and saturation magnetization, M_s. The soft material is thicker than a domain wall width, δ_{DW}, so while the interfacial spins remain coupled to the direction of the cobalt moments, a domain wall is created in the soft material parallel to the interface when a reverse field is applied. This wall allows much or all of M_s to be parallel to the applied field without breaking the moment coupling at the interface. In this case the field energy $2M_sH_{ex}t_a$ per unit interface area only has to be enough to create the domain wall of energy per unit area $\sigma_{DW} \approx 4\sqrt{(A\ Ku)}$ in the amorphous alloy. Hence M_s H_{ex} $(t_a - 2\delta_{DW}) = 4\sqrt{(A\ Ku)}$ giving $H_{ex} \approx 0.1$ Oe using $A = 10^{-6}$ erg/cm, $Ku = 10^3$ erg/cm^3, $M_s = 800$ Gauss and $t_s = 20$ microns. So this equation gives a reasonable number for the largest observed exchange field.

Further details of the microstructure of these samples will be published elsewhere[4].

REFERENCES

1. R.D. Heidenreich, E.A. Nesbitt, and R.D. Burbank, "Magnetic annealing in Perminvar. I. Structural origin," J. Appl. Phys., vol 30, pp. 995-1000, July 1959.; E.A. Nesbitt, R.D. Heidenreich, and A.J. Williams, "Soft magnetic materials : A necessary factor for heat treatment of the permalloys in a magnetic field," J. Appl. Phys., vol 31, pp. 228S-229S, May 1960.

2. E.A. Nesbitt, B.W. Batterman, L.D. Fullerton, and A.J. Williams, "Effect of oxygen on the magnetic and long range ordering properties of Ni3Fe," J. Appl. Phys.vol 36, pp. 1235-1236, March 1965.

3. D. Mauri, E. Kay, D. Scholl, and J.K. Howard, "Novel method for determining the anisotropy constant of MnFe in a NiFe/MnFe sandwich," J. Appl. Phys., vol 62, pp. 2929-2932, 'Ctober 1987.

4. C. K. Kim and R. C. O'Handley, "New Mechanism for Field Induced Anisotropy of Cobalt-rich Amorphous Alloys", Journal of Microscopy, Vol. 180, Pt 1, p.70-79, 1995.